Autophagy inhibition reduces irradiation-induced subcortical white matter injury not by reducing inflammation, but by increasing mitochondrial fusion and inhibiting mitochondrial fission

Yafeng Wang
Zhengzhou University
Yiran Xu
Zhengzhou University
Kai Zhou
Karolinska Institute: Karolinska Institutet
Yong Wang
University of Gothenburg: Goteborgs Universitet
Tao Li
Zhengzhou University
Cuicui Xie
Karolinska Institutet
Shan Zhang
Zhengzhou University
Xiaoli Zhang
Zhengzhou University
Juan Song
Zhengzhou University
Changlian Zhu (changlian.zhu@neuro.gu.se)
Zhengzhou University https://orcid.org/0000-0002-5029-6730

Research

Keywords: Autophagy, microglia, astrocyte, white matter injury, mitochondria, fusion and fission

Posted Date: February 24th, 2021

DOI: https://doi.org/10.21203/rs.3.rs-223625/v1

Version of Record: A version of this preprint was published at Molecular Neurobiology on December 28th, 2021. See the published version at https://doi.org/10.1007/s12035-021-02653-x.

Abstract

Background

Radiotherapy is an effective tool in the treatment of malignant brain tumors, but irradiation-induced late-onset toxicity remains a major problem. The purpose of this study was to investigate if genetic inhibition of autophagy has impact on subcortical white matter development in the juvenile mouse brain after irradiation.

Methods

Ten-day-old selective *Atg7* knockout (KO) mice and wild-type (WT) littermates were subjected to a single 6 Gy dose of whole-brain irradiation and evaluated at 5 days after irradiation.

Results

Neural *Atg7* deficiency partially prevented myelin disruption compared to the WT mice after irradiation, as indicated by myelin basic protein staining. Irradiation induced oligodendrocyte progenitor cell loss in the subcortical white matter, and *Atg7* deficiency partly prevented this. There was no significant change between the KO and WT mice in the number of microglia and astrocytes in the subcortical white matter after irradiation. Transcriptome analysis showed there were numbers of differentially expressed genes (DEGs) in both *Atg7* KO and WT group after irradiation, but GSEA analysis showed that the GO mitochondrial gene expression pathway was significantly enriched in the remaining DEGs between the KO and WT group after irradiation. Compared with WT mice, expression of the mitochondrial fusion protein OPA1 and phosphorylation of the mitochondrial fission protein DRP1 were dramatically decreased in KO mice under physiological conditions. The protein levels of phosphorylated DRP1 and OPA1 showed no differences in WT mice between the non-irradiated group and the irradiated group but had remarkably increased level in the KO mice after irradiation.

Conclusions

These results indicate that inhibition of autophagy reduces irradiation-induced subcortical white matter injury not by reducing inflammation, but by increasing mitochondrial fusion and inhibiting mitochondrial fission.

Background

Radiotherapy is an effective method for the treatment of malignant brain tumors in children; however, although the tumor cells are killed, such treatments can also damage normal brain tissue [1]. The developing brain in young children is much more sensitive to radiotherapy compared to the adult brain,

and it is more prone to long-term complications such as cognitive impairment, endocrine hormone disorders, and secondary malignant tumors, which severely reduces the long-term quality of life in childhood survivors of malignant brain tumors [2–4]. Irradiation-induced brain injury consists of a series of pathophysiological changes that take place after neural cells and intracranial blood vessels are injured by radiotherapy. Studies have found that even when low-to-medium-dose irradiation is administered, more than 30% of children have delayed mental or behavioral development [5]. Therefore, the prevention of neural cell death induced by radiotherapy and its long-term complications is an urgent clinical issue.

Autophagy is essential for survival, differentiation, development, and homeostasis by removing damaged and harmful components in cells. However, the inappropriate activation of autophagy is involved in cell death in the immature brain and is associated with childhood neurological disorders [6]. In our previous study, we showed that selective inhibition of autophagy in neural cells reduces irradiation-induced oligodendrocyte progenitor cell (OPC) loss. However, how deficiency in autophagy prevents white matter injury after irradiation is still not clear, and further research is needed.

The aim of this study was to investigate how the genetic inhibition of autophagy in the juvenile mouse brain impacts irradiation-induced subcortical white matter injury. We found that selective neural autophagy inhibition reduced irradiation-induced subcortical white matter injury not by reducing inflammation, but by increasing mitochondrial fusion and inhibiting mitochondrial fission.

Materials

Animals and ethical permission

Floxed *Atg7* mice were characterized as previously described [6, 7] and were crossed with a nestin-Cre-driven line to produce $Atg7^{flox/flox;\,Nes\text{-}Cre}$ knockout (*Atg7* KO) and $Atg7^{flox/+;\,Nes\text{-}Cre}$ mice (WT). All of the mice were housed in a temperature-controlled and pathogen-free environment with a 12:12-hour light-dark cycle. The genotyping of the pups was as described previously [6]. All experiments were approved by the animal research ethics committee (Gothenburg Committee of the Swedish Agricultural Agency) in accordance with national animal welfare legislation (2200-19).

Irradiation procedure

Postnatal day 10 (P10) *Atg7* KO and WT littermate pups of both sexes were anesthetized with a 50 mg/kg intraperitoneal injection of tribromoethanol (Avertin, Sigma-Aldrich, Stockholm, Sweden) and placed in a prone position (head to gantry) on a Styrofoam bed. The irradiation of the animals was performed using a linear accelerator (Varian Clinac 600CD; Radiation Oncology System LLC, San Diego, CA, USA) with 4 MV nominal photon energy and a dose rate of 2.3 Gy/min. The whole brain was irradiated with a single dose of 6 Gy to each mouse. The source-to-skin distance was approximately 99.5 cm. The head was covered with a 1 cm tissue-equivalent bolus material to obtain an even irradiation dose throughout the underlying tissue. After irradiation, the pups were returned to their dams and sacrificed at 5 days after irradiation. The sham-irradiated controls were anesthetized but not irradiated.

Immunohistochemistry staining

The mouse pups were deeply anesthetized with 50 mg/ml phenobarbital and perfused intracardially with phosphate buffered saline (PBS) and 5% buffered formaldehyde (Histofix; Histolab, Gothenburg, Sweden) at 5 days after irradiation. Brains were removed and fixed in 5% buffered formaldehyde at 4°C for 24 h. After dehydration with graded ethanol and xylene, the brains were paraffin-embedded and cut into 5 μm sagittal sections. Every 50th section from one hemisphere was deparaffinized in xylene and rehydrated in graded ethanol concentrations and stained for myelin basic protein (MBP), platelet derived growth factor receptor α (PDGFRα), ionized calcium-binding adaptor molecule 1 (Iba-1), and glial fibrillary acidic protein (GFAP). Antigen retrieval was performed by heating the sections in 10 mM boiling sodium citrate buffer (pH 6.0) for 10 min. Nonspecific binding was blocked for 30 min with 4% donkey or goat serum in PBS for 30 min. The primary antibodies were mouse anti-MBP (1:1,000 dilution, BioLegend, SMI 94, 836504), rabbit anti-PDGFRα (1:400 dilution, Cell Signaling, 3164), rabbit anti-Iba-1 (1:200 dilution, Wako Pure Chemical Industries, Ltd, 019-19741), and mouse anti-GFAP (1:250 dilution, Cell Signaling, 3670). After incubating the sections with the primary antibodies overnight at 4°C, the appropriate biotinylated secondary antibodies (1:200 dilution; all from Vector Laboratories, Burlingame, CA, USA) were added and incubated for 60 min at room temperature. After blocking endogenous peroxidase activity with 3% H_2O_2 for 10 min, the sections were visualized with Vectastain ABC Elite (Vector Laboratories) and 0.5 mg/mL 3,3’-diaminobenzidine enhanced with ammonium nickel sulfate, beta-D glucose, ammonium chloride, and beta-glucose oxidase. After dehydrating with graded ethanol and xylene, the sections were mounted using Vector mounting medium.

Cell quantification in mice

Iba-1, PDGFRα, and GFAP-positive cells were counted in the subcortical white matter under a stereo microscope (MicroBrightField, Magdeburg, Germany). The counting area in the subcortical white matter was traced, and the number of cells was expressed as cells/mm^2 [7, 8]. The counting was performed by a person who did not have prior knowledge of the groups. Three sections were counted with an interval of 250 μm between sections.

White matter injury evaluation and volume measurement

Four sections of each sample were used to measure the MBP-positive area using Micro Image (Olympus, Japan). The subcortical MBP-positive white matter volume (mm^3) was calculated as previously described [9] using the following formula: $V = SA \times p \times T$, where V is the total volume, SA is the sum of the areas measured, p is the inverse of the section sampling fraction, and T is the section thickness. To analyze cortical myelination as an indication of myelinated axons, the length of myelinated fibers within the cortex was measured between the end of myelinated axons and the cortical plate at fixed levels using the ImageJ software [9]. The immunodensity of MBP-positive staining in the myelinated axons was determined using the ImageJ software and manually setting the threshold to include the MBP-stained area, followed by measuring the proportion of the field that was positive for MBP staining in the

subcortical white matter. The MBP immunodensity was determined by measuring the integrated density and normalizing it to the WT non-irradiation group [7, 9].

RNA isolation, cDNA synthesis, and RNA sequencing

Samples of subcortical white matter from WT and KO mice after irradiation at 5 days and from the non-irradiated group were prepared for RNA isolation and RNA sequencing. Total RNA was isolated using the RNeasy mini kit (Qiagen, 74104) according to the manufacturer's instructions. The concentration and purity of all RNA samples were determined using a Nanodrop spectrophotometer (Nanodrop Technologies, Wilmington, DE, USA). The integrity of RNA was measured using the Experion RNA StdSens analysis kit (Bio-Rad, 7007103) on an Automated Electrophoresis Station (Bio-Rad, Hercules, CA, USA). One microgram of total RNA was reverse transcribed using the QuantiTect Reverse Transcription kit (Qiagen, 205311).

The library was prepared using an MGI Easy™ mRNA Library Prep Kit (BGI, Wuhan, China) following the manufacturer's instructions. The sequencing library was used for cluster generation and sequencing on the BGISEQ-500 system (BGI) [10]. The DESeq method was used to screen for differences between the two groups according to the criterion of $p < 0.05$. GO term classification was performed using the cluster Profiler R package [11]. Using MITOCARTA 3.0 (https://www.broadinstitute.org/mitocarta/mitocarta30-inventory-mammalian-mitochondrial-proteins-and-pathways) as the reference genome for mitochondria-related genes.

Quantitative real time PCR

Quantitative real time PCR (qRT-PCR) was performed using a LightCycler 480 instrument (Roche Diagnostics, Germany) and the SYBR Green technique according to the manufacturer's instructions. The primers used in the qRT-PCR reactions were designed by Beacon Designer software (free trial, PREMIER Biosoft) and included the oligodendrocyte and myelin-related genes *Olig2* (sense: 5'-CGG TGG CTT CAA GTC ATC-3', antisense: 5'-GTC ATC TGC TTC TTG TCT TTC T-3'), *Cldn11* (sense: 5'-TGG CAT CAT CGT CAC AAC-3', antisense: 5'-AGC CCA GTT CGT CCA TTT-3'), *CNP* (sense: 5'-TCT ACT TTG GCT GGT TCC T-3', antisense: 5'-CTT CTC CTT GGG TTC ATC TC-3'), and *MBP* (sense: 5'-CCT CAC AGC GAT CCA AGT-3', antisense: 5'-CAA GGA TGC CCG TGT CTC-3'). The mitochondrial fusion and fission-related genes included *Opa1* (sense: 5'-CCT GTG AAG TCT GCC AAT-3', antisense: 5'-TTA GAG AAG AGA ACT GCT GAA AT-3'), *Drp1* (sense: 5'-TGC TCA GTA TCA GTC TCT TC-3', antisense: 5'-GGT TCC TTC AAT CGT GTT AC-3'), and *Fis1* (sense: 5'-ATG AAG AAA GAT GGA CTG GTA G-3', antisense: 5'-GGA TTT GGA CTT GGA GAC A-3'). The reference genes were *Sdha* (sense: 5'-TTG CCT TGC CAG GAC TTA-3', antisense: 5'-CAC CTT GAC TGT TGA TGA GAA T-3') and *B2m* (sense: 5'-CCG AAC ATA CTG AAC TGC TA-3', antisense: 5'-AGG ACA TAT CTG ACA TCT CTA CTT-3'). The relative mRNA expression levels were calculated by the method of geometric averaging of multiple internal control genes.

Multiplex cytokine/chemokine assay

Cytokines and chemokines were measured in subcortical white matter homogenate supernatant fractions at 5 days after irradiation. Protein concentrations were measured with the BCA protein assay (Sigma, A2058) using samples prepared according to the manufacturer's protocol. Levels of interleukin (IL)-1β, IL-2, IL-4, IL-6, IL-10, and keratinocyte-derived chemokine (KC) were measured simultaneously using the Luminex Multiplex Cytokine Assay (Merck Chemicals and Life Science AB). The results were normalized to the total amount of protein in the sample.

Immunoblotting

Protein concentration was determined using the bicinchoninic acid method. Subcortical white matter homogenate samples (65 µl) were mixed with 25 µl NuPAGE LDS 4× sample buffer (ThermoFisher Scientific, NP0007) and 10 µl reducing agent (ThermoFisher Scientific, NP0004) and heated at 70°C for 10 min. Samples were run on 4–12% NuPAGE Bis-Tris gels (Invitrogen) and transferred to reinforced nitrocellulose membranes (Bio-Rad). After blocking with 5% fat-free milk in TBST buffer (20 mM Tris, 150 mM NaCl, and 0.1% Tween 20, pH 7.6) for 60 min at room temperature, the membranes were incubated with the following primary antibodies: mouse anti-OPA1 (1:1000 dilution, mouse monoclonal antibody, 612606, BD bioscience), mouse anti-DRP1 (1:500 dilution, mouse monoclonal antibody, sc-271583, Santa Cruz Biotechnology), rabbit anti-phospho-DRP1 (Ser637) (1:1000 dilution, rabbit polyclonal antibody, 4867S, Cell signaling), rabbit anti-FIS1 (FL-152) (1:500 dilution, rabbit polyclonal antibody, sc-98900, Santa Cruz Biotechnology), or rabbit anti-Actin (1:200 dilution, rabbit polyclonal antibody, A2066, Sigma) overnight. After washing, the membranes were incubated with peroxidase-labeled goat anti-rabbit IgG antibody (1:2000 dilution, Vector, PI-1000) or peroxidase-labeled horse anti-mouse IgG antibody (1:4000 dilution, Vector, PI-2000). Immunoreactive species were visualized using the SuperSignal West Pico PLUS Chemiluminescent Substrate (ThermoFisher Scientific, 34580) and an LAS 3000 cooled CCD camera (Fujifilm, Japan).

Statistical analysis

The Statistical Package for the Social Sciences 17.0 (SPSS, IBM, NY, USA) was used for all analyses. Comparisons between groups were performed by Student's *t*-test, and data with unequal variance were compared with the Mann–Whitney U-test. Two-way ANOVA followed by a Bonferroni post hoc test was used for multiple comparison correction of data from more than two groups. Results are presented as means ± SEM, and $p < 0.05$ was considered statistically significant.

Results

Disruption of subcortical white matter development in mice after irradiation

Myelination was visualized in the hemispheres of the brain as indicated by MBP staining (Fig. 1A). Subcortical white matter volume was assessed as the MBP-positive volume, and the volume was significantly reduced in WT mice (0.90 ± 0.04 mm^3) after irradiation compared to *Atg7* KO mice (1.14 ±

0.06 mm^3) ($p = 0.037$) (Fig. 1B). The irradiated mice also showed significantly shorter myelinated fibers within the cortex compared to non-irradiated mice (Fig. 1C), but *Atg7* deficiency protected against the shortening of myelinated fibers after irradiation (the mean fiber length was 296.9 μm in KO mice vs. 194.7 μm in WT mice, $p = 0.003$, Fig. 1D). Further analysis of the MBP-positive immunodensity in the myelinated fibers within the cortex showed that *Atg7* deficiency caused less obvious myelin disruption compared to the WT littermates after irradiation (Fig. 1E-F) ($p = 0.016$).

Atg7 deficiency reduced irradiation-induced OPC loss

As a marker of OPCs, we used PDGFRα staining to determine the extent of irradiation-induced white matter injury [7]. PDGFRα-positive cells were located mainly in the subcortical white matter (Fig. 2A), and the numbers of PDGFRα-positive cells were much lower in both groups of mice after irradiation ($p < 0.001$). However, there were more PDGFRα-positive cells in the *Atg7* KO mice compared with WT mice at 5 days after irradiation ($p = 0.033$) (Fig. 2B). We also measured the mRNA expression of oligodendrocyte-related and myelin-related genes (Fig. 2C). *Olig2*, *Cldn11*, *CNP*, and *MBP* mRNA expression was slightly high in the *Atg7* KO mice compared to WT mice after irradiation, but there was no difference between *Atg7* KO and WT pups.

Microglia activation and astrocyte reactivity after irradiation

Microglia activation and astrocyte reactivity are related to chronic inflammation in the brain. GFAP-labeled cells, as an indicator of astrocytes, were observed in the subcortical white matter (Fig. 3A). The number of astrocytes was significantly reduced after irradiation, but there was no significant difference between KO and WT pups (Fig. 3B). Similarly, Iba-1 labeling, as a marker of microglia, was also significantly reduced at 5 days after irradiation but showed no significant difference between KO and WT pups (Fig. 3C-3D). We also measured the protein levels of IL-1β, IL-2, IL-4, IL-6, IL-10, and KC in the subcortical white matter and found no difference at 5 days after irradiation between the *Atg7* KO and WT groups (Fig. 3E).

Irradiation induces transcriptome alterations in the Atg7 KO and WT

To further investigate whether *Atg7* KO has an impact on the mRNA transcriptome under physiological conditions or after irradiation, the transcriptomes of six *Atg7* KO and WT mouse brain tissue samples from the subcortical white matter were determined by RNA sequencing. Even when using the relaxed criterion of $p < 0.05$, the data showed that 2,606 of the total of 17,747 genes were differentially expressed in WT irradiated mice compared to WT non-irradiated mice. Among these 2,606 genes, 1,274 were upregulated and 1,332 were downregulated (Fig. 4A). For *Atg7* KO mice, the data analysis showed that 5,365 of the total of 20,753 genes were differentially expressed in irradiated group compared to non-irradiated group. Among these 5,365 genes, 2,916 were upregulated and 2,449 were downregulated (Fig. 4B). To compare the irradiation induced differentially expressed genes (DEGs) between WT and *Atg7* KO mice, Venn plot analysis was performed, and 1,931 DEGs were found in both WT and *Atg7* KO mice after irradiation (Fig. 4C). Gene ontology (GO) term classification was performed on the 1,931 DEGs in

three ontologies (molecular biological function, cellular component, and biological process) (Fig. 4D). Among the top eight classified GO terms according to the *p* adjust value, we found that most of the terms were non-specific, but some of them were related mitochondria.

Irradiation induces changes in the expression of mitochondria-related genes

Previous studies showed that mitochondria-related genes are more likely to specifically be involved in irradiation-induced brain injury [12, 13], and 1109 mitochondria-related genes in both KO and WT mice under physiological conditions or after irradiation were identified using MITOCARTA 3.0 (Fig. 5A). For further comparing the mitochondria-related gene expression between the KO and WT groups after irradiation, GSEA analysis showed significant differences ($p = 0.018$) in the DEGs in the GO Mitochondria gene expression pathway (Fig. 5B). Correlation analysis was performed for mitochondrial fusion (*Mfn1*, *Mfn2*, *Opa1*, and *Opa3*) and fission (*Drp1*, *Fis1*, *Mff*, and *Mief1*) related genes and for oligodendrocyte and myelin-related genes (*Cldn11*,*CNP*, *MBP*, *Olig2*) (Fig. 5C). The correlation heatmap showed that the *Cldn11*, *CNP*, and *MBP* genes had more negative correlations with mitochondrial fusion and fission genes, while the *Olig2* gene had more positive correlations with mitochondrial fusion and fission genes.

Effect of Atg7 deficiency on mitochondrial fission and fusion after irradiation

Based on the degree of correlation between mitochondrial fusion-fission genes and oligodendrocyte-myelin genes, the expression levels of *Opa1*, *Drp1*, and *Fis1* were confirmed by qRT-PCR. The expression of *Opa1*, *Drp1*, and *Fis1* was reduced after irradiation, but there were no significant differences between KO and WT either under physiological conditions or after irradiation (Fig. 6A). Western blot was performed to confirm the protein levels of OPA1, DRP1, and FIS1 (Fig. 6B), and the quantitative protein expression showed that the OPA1 protein level was significantly reduced in KO mice compared with WT mice in the non-irradiated groups ($p < 0.01$), while in the irradiated groups the OPA1 protein expression was higher in WT mice. However, WT mice after irradiation expressed less OPA1 protein at 100 kDa and 82 kDa, and a similar level at 75 kDa, while KO mice after irradiation expressed less OPA1 protein at 100 kDa, but higher protein levels at 82 kDa and significantly increased levels at 75 kDa ($p = 0.047$) (Fig. 6C).

Phosphorylated DRP1 (P-DRP1)at ser637 by protein kinase A had been shown to cause a significant decrease in GTPase activity and to inhibit mitochondrial fission [14, 15]. Compared with WT mice the abundance of P-DRP1 in KO mice was significantly decreased under physiological conditions ($p < 0.01$) but only slightly reduced after irradiation. Interestingly, the level of P-DRP1 showed no difference in WT mice between the non-irradiated group and the irradiated group, but was sharply increased in KO mice after irradiation ($p = 0.004$) (Fig. 6D). We found no difference in DRP1 or FIS1 protein levels (Fig. 6E-6F).

Discussion

Autophagy is a catabolic process that breaks down and recycles unnecessary or damaged cellular components, and it plays essential roles in development and in maintaining homeostasis in organisms [16]. As a classic autophagy-related gene, *Atg7* is crucial for the assembly and function of ubiquitin-like conjugates in the expansion of autophagosomal membranes [17]. Recent studies have shown that Atg7 is involved in the regulation of a variety of brain injury animal models [6, 18, 19], suggesting that Atg7 may be a target for therapeutic interventions. In our previous studies, we demonstrated that selective *Atg7* deletion prevents irradiation-induced caspase-3 activation, microglia activation, and inflammation and reduces irradiation-induced neural stem and progenitor cell death during the acute injury phase [8]. We also showed that selective inhibition of autophagy in neural cells reduces irradiation-induced subacute cerebellar white matter injury by decreasing OPC loss [7]. However, the mechanism through which autophagy deficiency prevents white matter injury after irradiation in the subacute injury phase is still unclear, and further research is needed. In this study, we showed that inhibition of autophagy reduces irradiation-induced subacute subcortical white matter injury not by reducing inflammation, but by increasing mitochondrial fusion and inhibiting mitochondrial fission.

Irradiation-induced brain injury is characterized by massive neural stem cell death followed by changes in cell metabolism, the cellular microenvironment, cell proliferation, and tissue shape as well as long-term cognitive impairments and growth reduction [20]. Studies of brain irradiation in animals have demonstrated the loss of myelin sheaths with apparent preservation of axons [21, 22], and this results in inhibited white matter development after irradiation as indicated by an up to 70% reduction in MBP staining [23]. Our previous study showed that *Atg7* deficiency reduced the severity of cerebellar white matter injury at 5 days after irradiation. In this study, subcortical white matter injury was evaluated by MBP staining at 5 days after irradiation, and *Atg7* deficiency resulted less obvious myelin disruption compared to WT littermates after irradiation, indicating that autophagy inhibition also reduced subcortical white matter injury in the juvenile mouse brain.

The proliferation and differentiation of OPCs is critical for the development of oligodendrocytes, and these cells undergo myelination throughout life, thus making them susceptible to irradiation insult [24]. OPC loss occurs in the acute phase after irradiation, and the numbers of OPCs are reduced significantly by 2–4 weeks after irradiation, but these numbers recover by 6 weeks after irradiation [25]. In the current study, we showed that the OPC loss in mice at 5 days after irradiation was significantly greater compared to non-irradiated mice, while *Atg7* deficiency reduced OPCs loss in the subcortical white matter after irradiation. These results indicate that deficiency in neural autophagy protects against radiation-induced subcortical white matter injury by preventing OPCs loss.

Microglia are the resident phagocytes of the central nervous system, and they are involved in the maintenance of brain homeostasis and immune defense [26]. Astrocytes play important roles in maintaining the homeostasis of ions, transmitters, water, and blood flow that is critical for the proper functioning of neural circuits [27]. Microglia activation and astrocyte reactivity are related to inflammation in the brain after cerebral insults, which cause the release of inflammatory chemokines and cytokines resulting in long-lasting chemical inflammatory brain injury [28, 29]. In this mouse model, we

found that the number of microglia and astrocytes decreased sharply at 5 days after irradiation, but there were no differences in the irradiated brain between *Atg7* KO and WT mice. Inflammation markers, as indicated by cytokines and chemokine levels were not significantly different between irradiated and non-irradiated mice or between *Atg7* KO and WT control littermates at this time point. These results suggest that microglia and astrocytes do not play a key role in irradiation-induced subcortical white-matter injury in this mouse model.

To further investigate the mechanism through which *Atg7* deficiency prevents subcortical white matter injury, we performed a transcriptome analysis. A total of 1105 DEGs were under physiological conditions, but only 160 DEGs were after irradiation, indicating that irradiation had a great impact on transcriptome activity in the juvenile brain. Previous studies showed that irradiation might lead to metabolic alterations in mitochondria, and thus mitochondria-related genes are more likely to be specifically involved in irradiation-induced brain injury [12, 13]. In addition, mitochondria are dynamic organelles that produce energy and molecular precursors that are essential for myelin synthesis, and thus the regulation of mitochondrial dynamics is likely to be important in the physiology and pathology of myelinated axons [30]. We therefore analyzed all of the mitochondria-related genes in the both KO and WT mice under physiological conditions and after irradiation, and we found that DEGs in the GO Mitochondria gene expression pathway showed significant differences between the KO and WT groups after irradiation, and subsequent correlation analysis showed that oligodendrocyte and myelin-related genes were correlated with mitochondria fusion and fission genes. These results suggest that mitochondria fusion and fission might be a crucial target for irradiation-induced white matter injury.

Mitochondria are dynamic organelles that constantly change shape as a result of a balance between fusion and fission, and modulating the balance of mitochondrial fission–fusion is crucial for maintaining cellular homeostasis [31]. Irradiation results in nuclear DNA damage, and there is evidence suggesting that such nuclear damage occurs secondary to mitochondrial injury [32]. Due to the lack of protection by proteins and histones, mitochondria are very susceptible to irradiation damage [33]. As a result, compensatory mitochondrial fusion after low-dose irradiation is needed to remove the dysfunctional mitochondrial DNA and to maintain respiratory function [34]. At medium or high-dose irradiation, mitochondrial fusion usually decreases [35]. Protein kinase A phosphorylates DRP1 at ser637 in the conserved GTPase effector domain of rodent animals, and this phosphorylation had been revealed cause a significant decrease in GTPase activity and to inhibit mitochondrial fission [14, 15]. P-DRP1, as a marker of inhibited mitochondrial fission, showed the same tendency as the mitochondria fusion marker OPA1. In this study, their protein levels dramatically decreased in KO mice compared with WT mice under physiological conditions, and the loss of selective autophagy led to decreased mitochondria fusion. Although the differences were significant under physiological conditions, there was no significant change under physiological conditions in the myelin sheath between KO and WT mice as Fig. 1 described. Interestingly, the protein levels of P-DRP1 and OPA1 showed no differences in WT mice between the non-irradiated group and the irradiated group, but they were significantly increased in KO mice after irradiation at 5 days after irradiation. We assumed that autophagy deficiency in the KO mice might reduce the sensitivity of mitochondria to irradiation by increasing mitochondrial fusion and inhibiting mitochondrial

fission after irradiation, and thus providing more energy and molecular precursors for myelin synthesis. These results suggest that autophagy inhibition prevents irradiation-induced subcortical white matter injury by increasing mitochondrial fusion and inhibiting mitochondrial fission.

Conclusions

In conclusion, selective neural *Atg7* KO reduced irradiation-induced subcortical white matter injury by increasing mitochondrial fusion and inhibiting mitochondrial fission in the juvenile mouse brain. Further studies are needed to clarify the mechanism behind these effects. Our study suggests that inhibition of neural autophagy might be a potential therapeutic target for irradiation-induced brain injury in children being treated for malignant brain tumors.

Abbreviations

MBP
myelin basic protein
OPC
oligodendrocyte progenitor cell
Atg7
autophagy 7
PDGFRα
platelet derived growth factor receptorα
GFAP
glial fibrillary acidic protein
Iba-1
calcium-binding adaptor molecule 1
WT
wild-type
KO
knockout
DEG
differentially expressed gene
FIS1
Mitochondrial fission 1 protein
DRP1
dynamin-related protein 1
IL
Interleukin
KC
keratinocyte-derived chemokine

Declarations

Acknowledgements

Not applicable.

Funding

This work was supported by National Natural Science Foundation of China (82003396, U1704281), the Swedish Cancer Foundation (CAN2017/509, 20-1121-PjF), the Swedish Childhood Cancer Foundation (PR2018-0082), the governmental grants to scientists working in health care in Gothenburg (ALFGBG-717791).

Authors' contributions

YW, YX and KZ performed the experiments, analyzed the data, and wrote the manuscript. YW, YX, TL, CX, and SZ performed the experiments and analyzed the data. XZ and JS analyzed the data. CZ designed the study, analyzed the data, and revised the manuscript. All of the authors read and approved the final manuscript.

Availability of data and materials

All data generated or analyzed during this study are included in the published article.

Ethics approval and consent to participate

The study was approved by the animal research ethics committee (Gothenburg Committee of the Swedish Agricultural Agency) in accordance with national animal welfare legislation (2200-19).

Consent for publication

Not applicable.

Competing interests

The authors declare that they have no competing interests.

References

1. Baron Nelson M, Compton P, Patel SK, Jacob E, Harper R. Central nervous system injury and neurobiobehavioral function in children with brain tumors: a review of the literature. Cancer nursing. 2013;36:E31-47.

2. Zajac-Spychala O, Pawlak MA, Karmelita-Katulska K, Pilarczyk J, Derwich K, Wachowiak J. Long-term brain structural magnetic resonance imaging and cognitive functioning in children treated for acute

lymphoblastic leukemia with high-dose methotrexate chemotherapy alone or combined with CNS radiotherapy at reduced total dose to 12 Gy. Neuroradiology. 2017;59:147-56.

3. Rose SR, Horne VE, Howell J, Lawson SA, Rutter MM, Trotman GE, et al. Late endocrine effects of childhood cancer. Nature reviews Endocrinology. 2016;12:319-36.

4. Paulino AC, Fowler BZ. Secondary neoplasms after radiotherapy for a childhood solid tumor. Pediatric hematology and oncology. 2005;22:89-101.

5. Anderson NE. Late complications in childhood central nervous system tumour survivors. Current opinion in neurology. 2003;16:677-83.

6. Xie C, Ginet V, Sun Y, Koike M, Zhou K, Li T, et al. Neuroprotection by selective neuronal deletion of Atg7 in neonatal brain injury. Autophagy. 2016;12:410-23.

7. Wang Y, Zhou K, Li T, Xu Y, Xie C, Sun Y, et al. Selective Neural Deletion of the Atg7 Gene Reduces Irradiation-Induced Cerebellar White Matter Injury in the Juvenile Mouse Brain by Ameliorating Oligodendrocyte Progenitor Cell Loss. Frontiers in cellular neuroscience. 2019;13:241.

8. Wang Y, Zhou K, Li T, Xu Y, Xie C, Sun Y, et al. Inhibition of autophagy prevents irradiation-induced neural stem and progenitor cell death in the juvenile mouse brain. Cell death & disease. 2017;8:e2694.

9. Zhang X, Rocha-Ferreira E, Li T, Vontell R, Jabin D, Hua S, et al. gammadeltaT cells but not alphabetaT cells contribute to sepsis-induced white matter injury and motor abnormalities in mice. Journal of neuroinflammation. 2017;14:255.

10. Li T, Li K, Zhang S, Wang Y, Xu Y, Cronin SJF, et al. Overexpression of apoptosis inducing factor aggravates hypoxic-ischemic brain injury in neonatal mice. Cell death & disease. 2020;11:77.

11. Yu G, Wang LG, Han Y, He QY. clusterProfiler: an R package for comparing biological themes among gene clusters. Omics : a journal of integrative biology. 2012;16:284-7.

12. Sharma NK, Stone S, Kumar VP, Biswas S, Aghdam SY, Holmes-Hampton GP, et al. Mitochondrial Degeneration and Autophagy Associated With Delayed Effects of Radiation in the Mouse Brain. Frontiers in aging neuroscience. 2019;11:357.

13. Kempf SJ, Moertl S, Sepe S, von Toerne C, Hauck SM, Atkinson MJ, et al. Low-dose ionizing radiation rapidly affects mitochondrial and synaptic signaling pathways in murine hippocampus and cortex. Journal of proteome research. 2015;14:2055-64.

14. Knott AB, Perkins G, Schwarzenbacher R, Bossy-Wetzel E. Mitochondrial fragmentation in neurodegeneration. Nature reviews Neuroscience. 2008;9:505-18.

15. Chang CR, Blackstone C. Cyclic AMP-dependent protein kinase phosphorylation of Drp1 regulates its GTPase activity and mitochondrial morphology. The Journal of biological chemistry. 2007;282:21583-7.

16. Shimizu S. Biological Roles of Alternative Autophagy. Molecules and cells. 2018;41:50-4.

17. Xiong J. Atg7 in development and disease: panacea or Pandora's Box? Protein & cell. 2015;6:722-34.

18. Wang HJ, Wei JY, Liu DX, Zhuang SF, Li Y, Liu H, et al. Endothelial Atg7 Deficiency Ameliorates Acute Cerebral Injury Induced by Ischemia/Reperfusion. Frontiers in neurology. 2018;9:998.

19. Shi H, Wang J, Huang Z, Yang Z. IL-17A induces autophagy and promotes microglial neuroinflammation through ATG5 and ATG7 in intracerebral hemorrhage. Journal of neuroimmunology. 2018;323:143-51.

20. Balentova S, Adamkov M. Molecular, Cellular and Functional Effects of Radiation-Induced Brain Injury: A Review. International journal of molecular sciences. 2015;16:27796-815.

21. Bull C, Cooper C, Lindahl V, Fitting S, Persson AI, Grander R, et al. Exercise in Adulthood after Irradiation of the Juvenile Brain Ameliorates Long-Term Depletion of Oligodendroglial Cells. Radiation research. 2017;188:443-54.

22. Panagiotakos G, Alshamy G, Chan B, Abrams R, Greenberg E, Saxena A, et al. Long-term impact of radiation on the stem cell and oligodendrocyte precursors in the brain. PloS one. 2007;2:e588.

23. Fukuda H, Fukuda A, Zhu C, Korhonen L, Swanpalmer J, Hertzman S, et al. Irradiation-induced progenitor cell death in the developing brain is resistant to erythropoietin treatment and caspase inhibition. Cell death and differentiation. 2004;11:1166-78.

24. Begolly S, Olschowka JA, Love T, Williams JP, O'Banion MK. Fractionation enhances acute oligodendrocyte progenitor cell radiation sensitivity and leads to long term depletion. Glia. 2018;66:846-61.

25. Atkinson SL, Li YQ, Wong CS. Apoptosis and proliferation of oligodendrocyte progenitor cells in the irradiated rodent spinal cord. International journal of radiation oncology, biology, physics. 2005;62:535-44.

26. Hu X, Leak RK, Shi Y, Suenaga J, Gao Y, Zheng P, et al. Microglial and macrophage polarization-new prospects for brain repair. Nature reviews Neurology. 2015;11:56-64.

27. Burda JE, Bernstein AM, Sofroniew MV. Astrocyte roles in traumatic brain injury. Experimental neurology. 2016;275 Pt 3:305-15.

28. Raffaele S, Lombardi M, Verderio C, Fumagalli M. TNF Production and Release from Microglia via Extracellular Vesicles: Impact on Brain Functions. Cells. 2020;9.

29. Karve IP, Taylor JM, Crack PJ. The contribution of astrocytes and microglia to traumatic brain injury. British journal of pharmacology. 2016;173:692-702.

30. Gonzalez S, Fernando R, Berthelot J, Perrin-Tricaud C, Sarzi E, Chrast R, et al. In vivo time-lapse imaging of mitochondria in healthy and diseased peripheral myelin sheath. Mitochondrion. 2015;23:32-41.

31. Fenton AR, Jongens TA, Holzbaur ELF. Mitochondrial dynamics: Shaping and remodeling an organelle network. Current opinion in cell biology. 2020;68:28-36.

32. Azzam EI, Jay-Gerin JP, Pain D. Ionizing radiation-induced metabolic oxidative stress and prolonged cell injury. Cancer letters. 2012;327:48-60.

33. Kam WW, Banati RB. Effects of ionizing radiation on mitochondria. Free radical biology & medicine. 2013;65:607-19.

34. Chen H, Vermulst M, Wang YE, Chomyn A, Prolla TA, McCaffery JM, et al. Mitochondrial fusion is required for mtDNA stability in skeletal muscle and tolerance of mtDNA mutations. Cell. 2010;141:280-9.

35. Gan L, Wang Z, Si J, Zhou R, Sun C, Liu Y, et al. Protective effect of mitochondrial-targeted antioxidant MitoQ against iron ion (56)Fe radiation induced brain injury in mice. Toxicology and applied pharmacology. 2018;341:1-7.

Figures

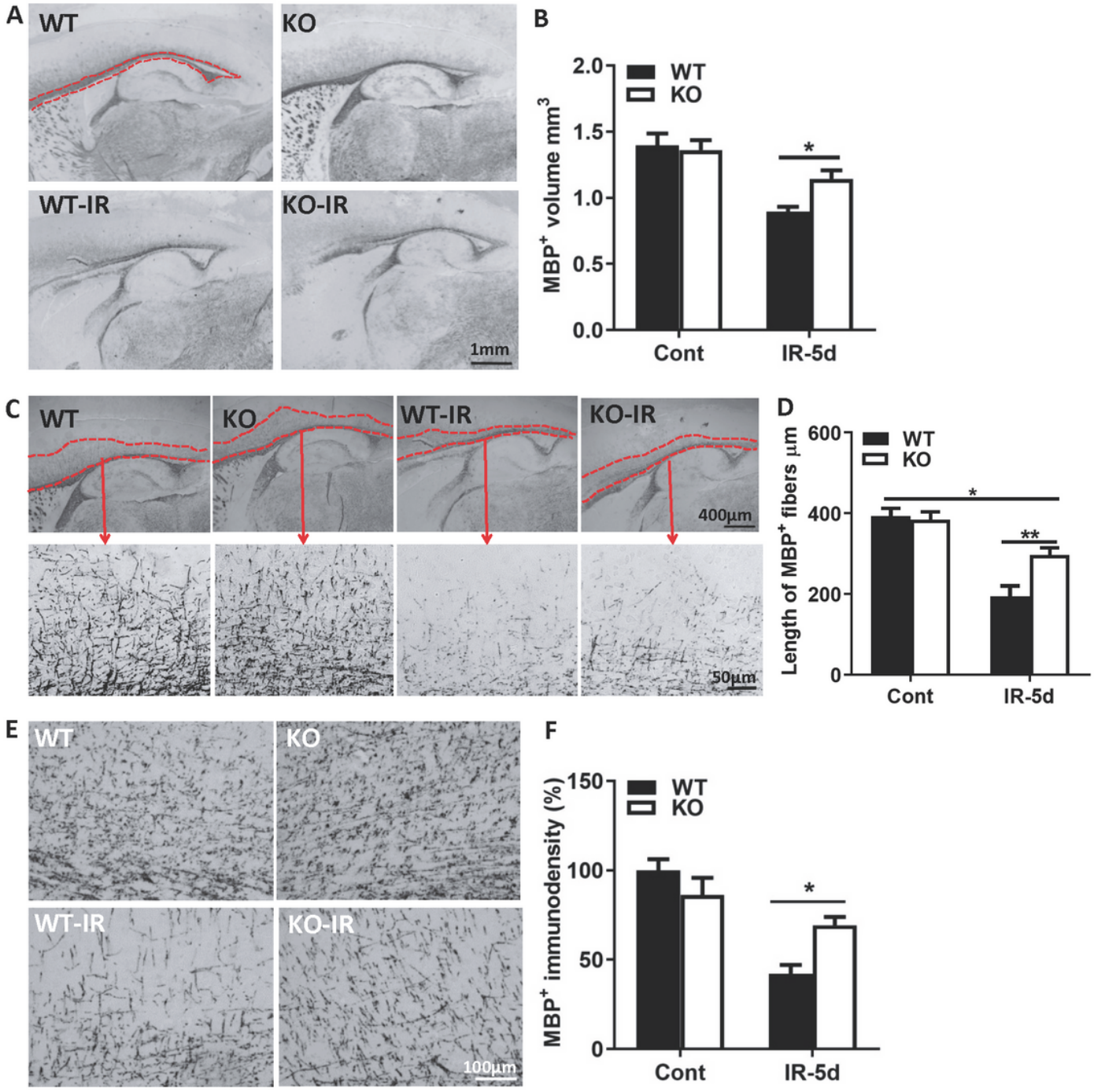

Figure 1

Cerebral radiation interrupted subcortical white matter development in young mice A. Representative sagittal hemisphere MBP staining in WT and Atg7 KO control and irradiated mouse pups. B. The subcortical white matter volume assessed as the volume of MBP-positive staining. Atg7 KO protected against the irradiation-induced reduction in subcortical white matter. C. Representative MBP staining in subcortical white matter and myelinated fibers. D. The mean lengths of MBP-positive myelinated fibers between the end of myelinated axons and the cortical plate at fixed levels. E. Representative MBP immunostaining in myelinated fibers within the cortex. F. The MBP-positive immunodensity in myelinated

fibers is presented as the percentage of controls. n = 7/group for the immunostaining. *p < 0.05, **p < 0.01.

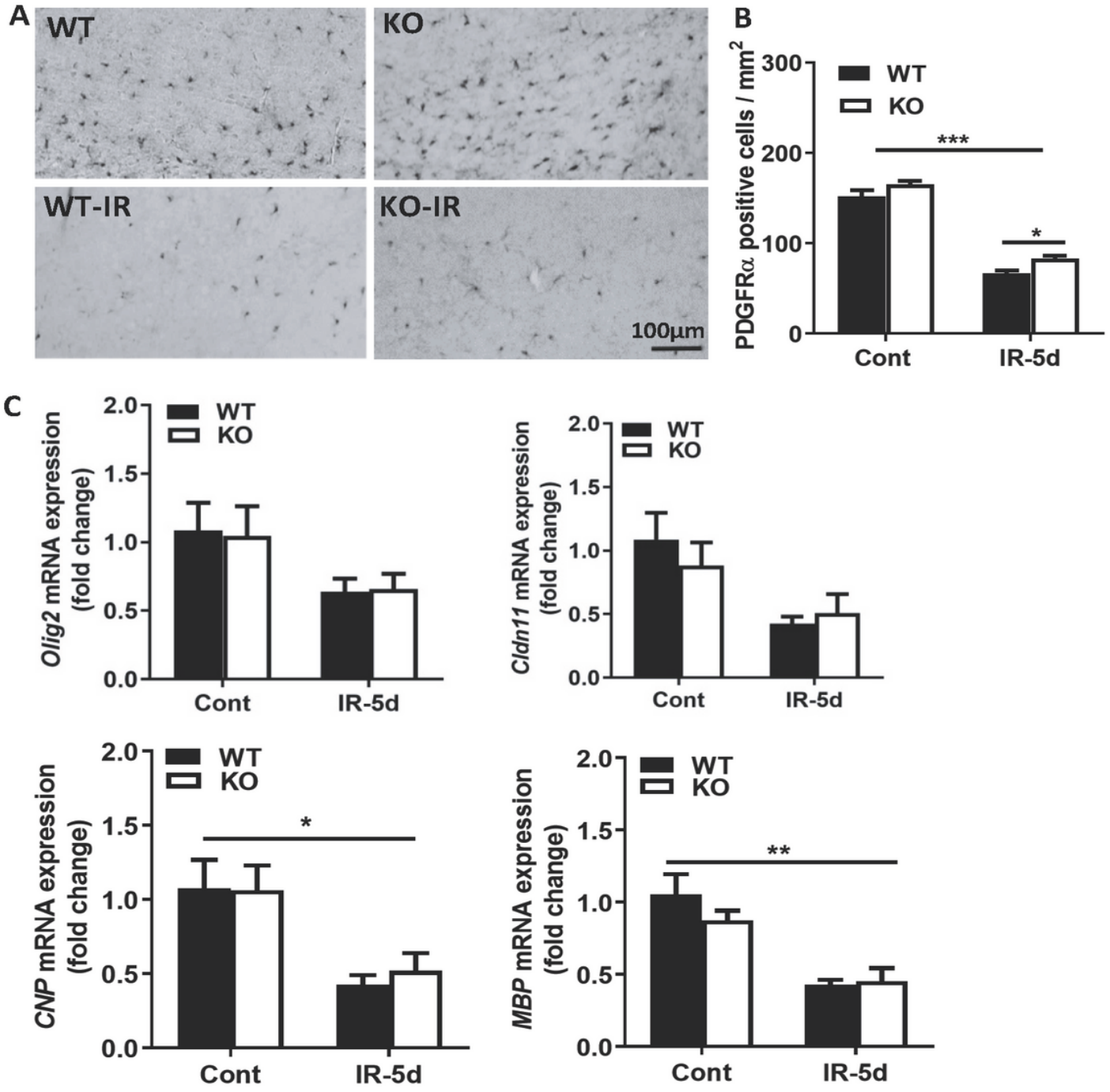

Figure 2

Atg7 KO reduced irradiation-induced OPC loss in the subcortical white matter A. Representative images of OPCs in the subcortical white matter after irradiation that were immunostained for PDGFRα in WT and Atg7 KO control and irradiated mouse pups. B. Quantitative analysis of the PDGFRα-labeled cells in the subcortical white matter. C. Bar graphs showing the mRNA expression of Olig2, Cldn11, CNP, and MBP in

the cortical tissue, including the subcortical white matter, at 5 days after irradiation. n = 7/group for the immunostaining, and n = 5/group for qRT-PCR. *p < 0.05, **p < 0.01, ***p < 0.001.

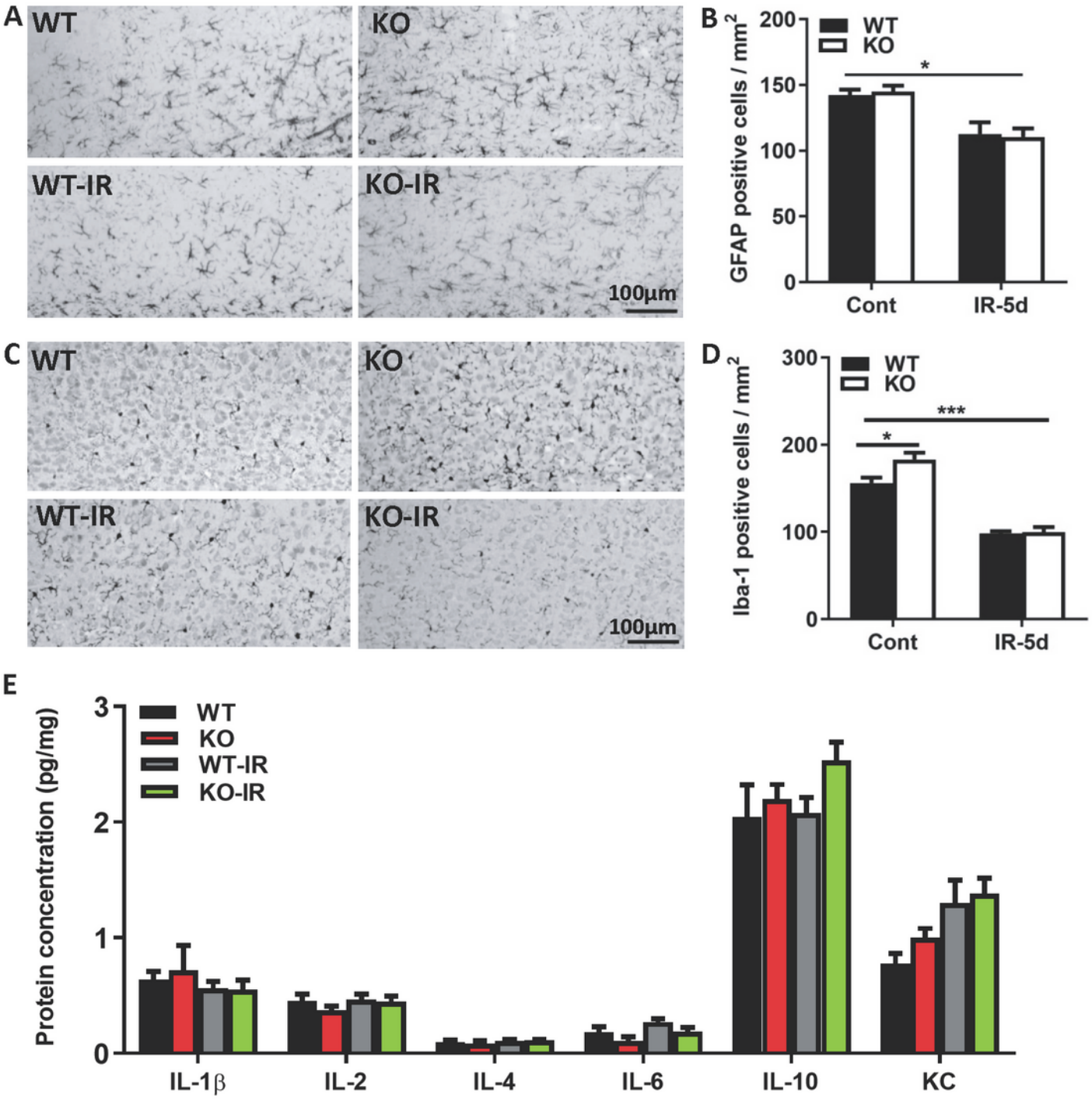

Figure 3

Astrocyte and microglia changes in the subcortical white matter after irradiation. A. Representative images of GFAP-labeled cells in the subcortical white matter. B. Quantification of GFAP-labeled cells in the subcortical white matter. C. Representative Iba-1 immunostaining in the subcortical white matter. D.

Quantification of Iba-1–labeled cells in the subcortical white matter. E. The protein levels of IL-1β, IL-2, IL-4, IL-6, IL-10, and KC in the cortical tissue at 5 days after irradiation were detected by Luminex assay in the Atg7 KO and WT pups. n = 7/group for the immunostaining and Luminex assay. *p < 0.05, ***p < 0.001.

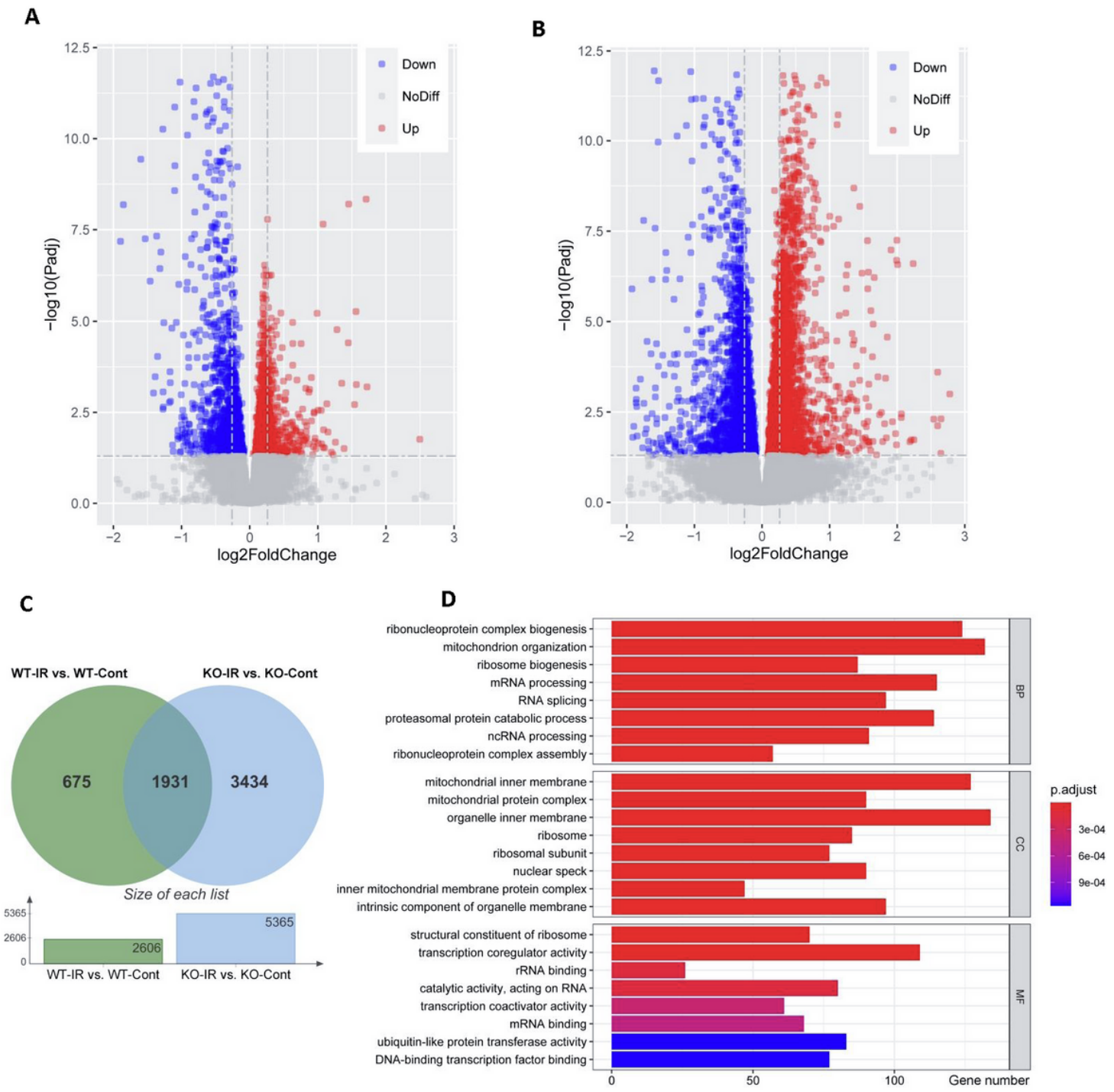

Figure 4

Irradiation induces transcriptome alterations in WT and Atg7 KO mice. A. Volcano plot showing DEGs between WT irradiated mice and WT non-irradiated mice in the subcortical white matter. B. Volcano plot

showing DEGs between KO irradiated mice and KO non-irradiated mice in the subcortical white matter. C. Venn plot showing the intersection of DEGs between Atg7 KO and WT mice after irradiation. D. The graph shows the top 8 classified GO terms in three ontologies. GO classification was performed based on the 1931 DEGs. The x-axis represents the number of DEGs, and the y-axis represents the GO terms. MF: molecular biological function; CC: cellular component; BP: biological process. n = 6/group for RNA sequencing.

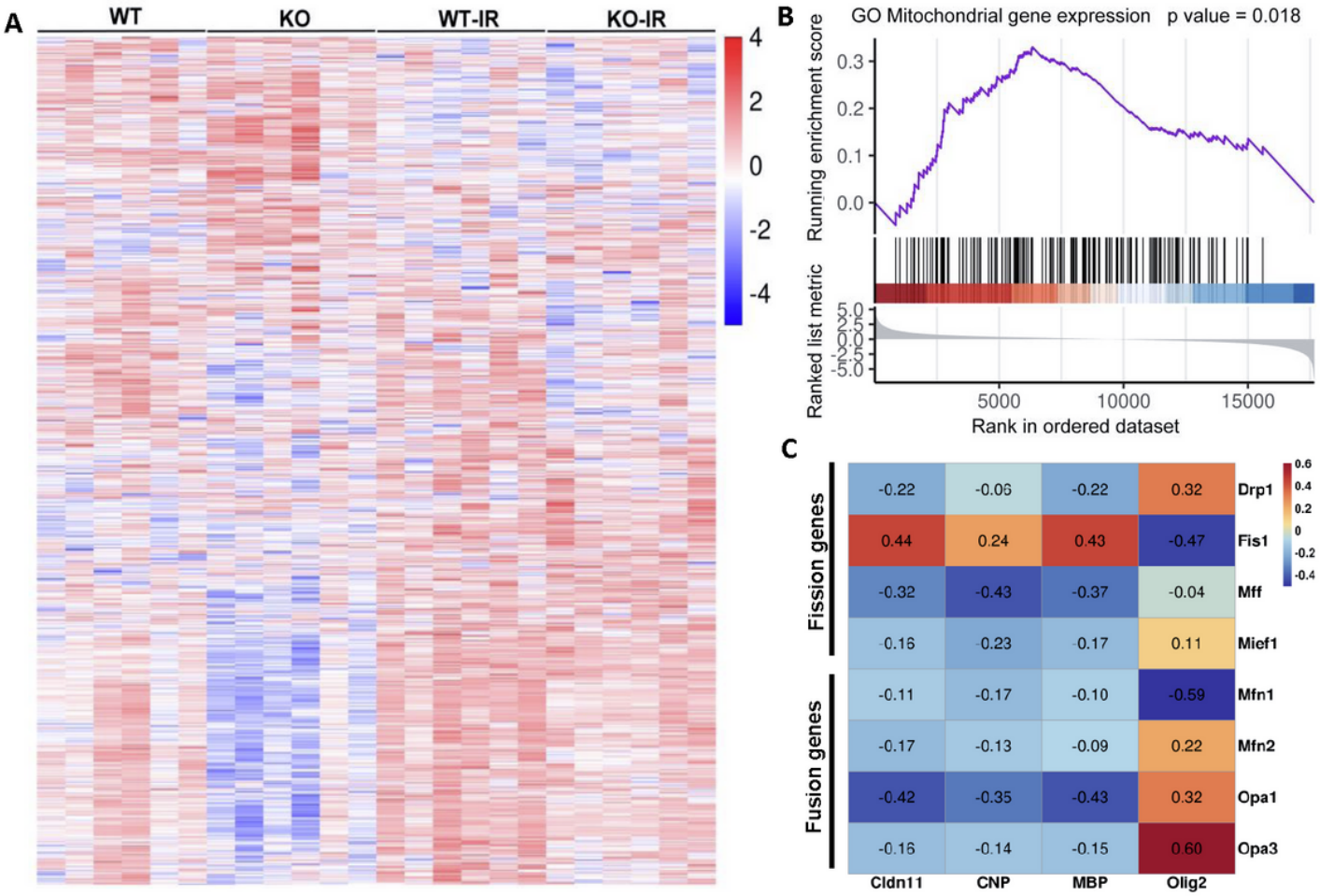

Figure 5

Irradiation induces mitochondria-related gene alterations. A. Heatmap of mitochondria-related DEGs. B. GSEA analysis showed DEGs in the GO mitochondrial genes expression pathway. C. Correlation heatmap for mitochondria fusion and fission-related genes and oligodendrocyte and myelin-related genes. Some genes were negatively related and others were positively related as represented in different colors. The number in the correlation heatmap is the correlation coefficient.

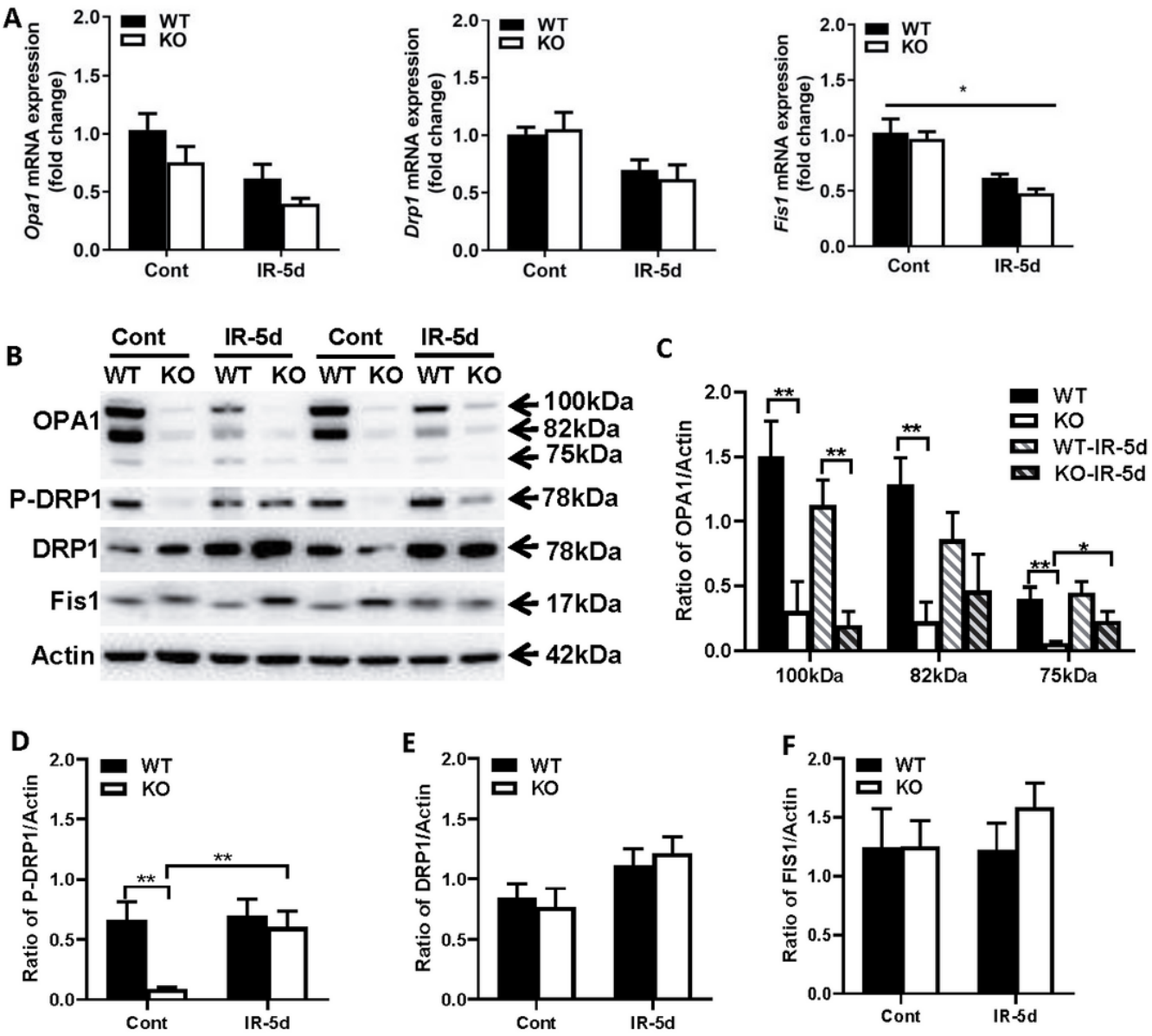

Figure 6

Effect of Atg7 deficiency on mitochondrial fission and fusion in the subcortical white matter after irradiation. A. Bar graphs showing mRNA expression of Opa1, Drp1, and Fis1 at 5 days after irradiation. B. Representative immunoblots of mitochondrial fusion protein (OPA1) and fission proteins (P-DRP1/DRP1 and Fis1) in WT and KO mice under physiological conditions and after irradiation. C-F. Quantification of OPA1, P-DRP1, DRP1, and FIS1. n = 5/group for qRT-PCR, n = 6/group for immunoblotting. *p < 0.05, **p < 0.01.